Journal of Wasit for Science and Medicine 2026: 19, (3), 107-122

Monitoring the Water Quality of Iraq Tigris River During the Winter and Spring Seasons Using Remote Sensing and Situ Measurements

Mutasim Ibrahim Malik

Department of Physics, College of Science, Wasit University, Kut, Iraq.

mutasim@uowasit.edu.iq

Abstract

This article contrasts situ measurements with data from remote sensing (RS) and geographic information systems (GIS) used to monitor the water quality parameters of the Tigris River in Wasit Governorate, Iraq. RS and GIS are essential for measuring and monitoring water quality parameters. The study examines seasonal differences between winter and spring in water quality parameters like temperature, pH, electrical conductivity (EC), dissolved oxygen (DO), BOD_5, total dissolved solids (TDS), total suspended solids (TSS), turbidity, total hardness (T.H), nitrate, phosphate, total organic matter (TOM), and chlorophyll-a. Station 12 had the highest mean water turbidity value in spring, exceeding the WHO critical limit. Chlorophyll-a concentrations varied, with the lowest mean value in winter and the highest in spring. The study used Landsat-9 data and Multiple Linear Regression (MLR) to predict certain water quality parameters, showing a strong correlation between Landsat-9 spectral reflectance data and selected parameters like turbidity, TOM, TDS, TSS, and chlorophyll-a. Landsat-9 spectral sensors can detect changes in water quality based on spectral reflectance characteristics. For turbidity, a significant correlation was observed with ($SWIR1_{L9}$, MNDWI, NDMI, C_{L9}/B_{L9}, B_{L9}/G_{L9}, and R_{L9}/B_{L9}) in winter and (NDMI, C_{L9}/B_{L9}, C_{L9}/G_{L9}, and B_{L9}/C_{L9}) In spring, achieving an R^2 value of 96% in winter and 53% in spring. For TDS, TSS, TOM, and chlorophyll-a, high R^2 values were also achieved in both seasons, with R^2 values ranging from 63% to 97% across different variables and parameters.

Keywords: Tigris River in Wasit Governorate - Iraq, Water quality parameters, RS, MLR, GIS.

1. Introduction

The problem of water scarcity has recently received wide attention due to harmful human activities and the unexpected consequences of climate change[1, 2]. Freshwater resources are then in the form of rivers or lakes, wetlands or swamps, reservoirs, water from premeditated wells, or artesian water [3]. Iraqi rivers face many difficulties in water quality. Rainfall levels are declining due to climate change, which affects water temperatures. Other factors, such as dams and irrigation operations, can be controlled[4]. Still, most of these impacts are associated with the activities of other nations, including Turkey and Iran. Hence, actions taken in various countries are central to determining water quality in Iraqi rivers 5]. Water quality parameters refer to the specific attributes of water that distinguish its thermal, chemical, physical, and biological aspects [6]. Water quality monitoring should be used to direct conservation efforts and enhance environmental quality to ascertain the state of aquatic systems in rivers and lakes [7]. Traditional river and lake water study methods have become expensive compared to the environmental data obtained [8].

The water quality is determined by taking samples from the site and testing them in the laboratory. Based on these findings, the study compares the results of this analysis with those of modern sensing technology to establish a relationship with water quality status [9]. Even if the data collected is accurate for a specific time in a particular area, it cannot be used to evaluate other places and times. For this reason, remote sensing and GIS are critical in thoroughly studying, examining, and assessing the water quality status[10]. As an example of remote sensing and GIS applications, satellite imagery has always stipulated the significance of water and its monitoring and management. The techniques of satellite remote sensing have been created for water quality and are commonly used in many water resource control tasks. Remote sensing is cheaper when compared to many field methods and has high spatial and temporal density over large areas [11]. Water quality attributes that may be sensed remotely include chlorophyll-a, water temperature, turbidity, TOM, and suspended sediment[12, 13]. Some common uses of the GIS include using distances and locations, quantities and densities, and changes in the system to enhance decision-making processes [14].

2. Materials and Method

2.1. Study site

The Tigris River passes through Wasit Governorate in Iraq, and its length in this governorate is about 136 kilometers. Wasit Governorate is located in central Iraq. It is bordered to the north by Diyala Governorate, to the northwest by the capital of Iraq (Baghdad), to the west by Babil Governorate, to the south by Al-Qadisiyah Governorate, to the southeast by Maysan Governorate, and to the east by the international border with Iran. The Tigris River is approximately 18 m above sea level in Wasit Governorate. The terrain is characterized by a flood plain, lowlands, water bodies and ponds, agriculture and irrigation. Water samples were collected from 12 stations over several months within the winter (4 December, 6 January, and 8

February) and spring (3 March, 4 April, and 14 May) of 2024 along the Tigris River Wasit Governorate Table 1. An image of the Tigris River and study station located at Wasit Governorate was captured by a Landsat-9 satellite, and the image enhancement was done using band 7, band 5 and band 1 to get the composite images as illustrated in Fig. 1[16].

Table 1. Geographic coordinates of the water sampling stations using GPS (Garmin 72H).

Station	Coordinates	
	Latitude (N)	Longitude (E)
St1	32°57'56.38"N	44°45'30.94"E
St2	32°55'30.42"N	44°48'26.63"E
St3	32°54'10.15"N	45° 3'21.02"E
St4	32°52'34.77"N	45° 4'36.86"E
St5	32°49'21.65"N	45° 2'58.77"E
St6	32°45'56.39"N	45°10'30.10"E
St7	32°34'55.46"N	45°24'55.74"E
St8	32°35'9.11"N	45°31'49.95"E
St9	32°32'44.10"N	45°42'6.89"E
St10	32°31'54.61"N	45°52'29.40"E
St11	32°39'19.90"N	46° 7'57.48"E
St12	32°33'21.91"N	46°17'49.51"E

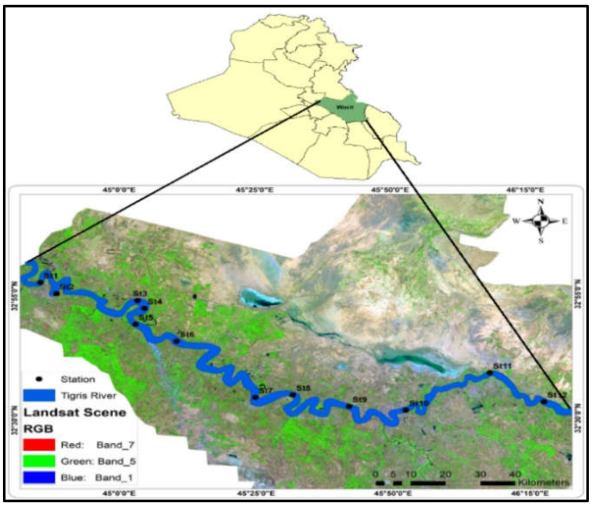

Figure 1. The Tigris River and stations in the study site.

2.2. Procedures of Sampling

Specimens were collected from the immediate vicinity of the water's surface (0.5 m) in order to analyze the particular parameters: Electrical Conductivity (EC), TSS, pH, Temperature, Total Organic Matter (TOM), Dissolved Oxygen (DO), BOD5, Turbidity, TDS, Nitrate, Phosphate, Total Hardness (T.H), and Chlorophyll-a. These parameters are collected simultaneously when a Landsat satellite image of the study area is taken. In the field, TDS, EC, temperature, and pH measurements were made with a portable Multimeter MARTINI instruments Model (Mi180 Bench Meter) and Multi-Parameter Meter Model (PH-2603). Tests were conducted following the unified standards set by the World Health Organization [17]. Turbidity was measured using a HACH.2100N turbidimeter. Additionally, a German-made Torch device was utilized to measure chlorophyll-a concentration for the study.

2.3. Remote sensing measurements

The study used remote sensing data from Landsat-9 (L1TP), which consists of two scene paths (167,168) and rows (38,37) . Tow images were acquired on 6 /January 2024 and 4 / April 2024.The study area images were acquired from the United States Geological Survey (USGS), which provides free satellite data and imagery access through an Internet-based search and sorting facility. The software for digitally manipulating Landsat-9 images is ArcGIS 10.8 and ENVI 5.3. The study area consists of two scenes, so the mosaic of the image was created before processing and analysis were carried out. This research used the World Geodetic System 1984 (WGS 84) projection.

We selected 24 Ground Control Points (GCPs) from the images and adjusted them to align with the Universal Transverse Mercator (UTM) system. Previous studies have shown that the geometric correction process requires 24 ground control points sufficient for the geometric correction of images. Using the nearest neighbour approach, the original images' digital numbers (DNs) values were preserved.[19].Since the atmosphere can affect images by absorbing, scattering and refraction light, samples were collected on days when there was no atmospheric influence, such as clouds, i.e., clear weather. Atmospheric correction uses top-of-atmosphere reflectance values (TOA) to alleviate the impact of the atmosphere and transform DNs into at-sensor reflectance values [20]. Sensor reflectance values were obtained by converting digital numbers (DNs) using ENVI 5.3 image processing software. The range of top-of-atmosphere reflectance values is between 0 and 1. This option is applicable when the image includes offsets, sun elevation, and solar irradiance. The program ENVI5.3 extracts these values from the metadata of the list of sensors. The following formula was utilized to calculate reflectance (P_λ) [12, 19, 21].

$$\mathbf{P_\lambda = \frac{\pi L_\lambda d^2}{ESUN_\lambda \sin\theta}} \quad (1)$$

Where: - L_λ = Radiance amount W/(m^2·sr·µm). d= Distance between Earth and Sun (Astronomical Unit). $ESUN_\lambda$= Solar irradiance W/(m^2·µm). θ= Sun altitude in degrees. The reflectance offsets and gains of Landsat-9 data have been adjusted according to the sun elevation sine. Next, the calculation of brightness temperature is performed using only thermal images from Landsat-9, TIRS-1, and TIRS-2, as they are compatible with this option. Using the Planck equation, we can calculate the brightness temperatures in degrees Celsius by reversing the process and converting the spectral irradiance to the surface temperature [12].

$$\mathbf{T = \frac{U_2}{\ln(\frac{U_1}{L_\lambda}+1)} - 273.15} \quad (2)$$

Where: - U_1 and U_2 = constants of calibration in kelvin. Moreover, 9 indices are created for vegetation and water ((MNDWI), (DVI), (NDMI), (AWEI), (NDVI), (RVI), (IPVI), (WRI), and (NDWI)). The use of band ratios in this study is aimed at lessening the effect of terrain and increasing the number of independent variables in the models. Extending band combinations enhances the differentiation of the spectra between the bands, hence mastering their effects. Band combinations in remote sensing are utilized to improve the differentiation of features, optimize information extraction, observe specific processes, highlight temporal dynamics, adapt data for particular sensors, and effectively reduce noise without interfering with target features. Merging one spectral band with another yields a picture with proportional band intensities. Spectral indices are mathematical formulas integrating surface reflectance data at two or more specified wavelengths to assess several significant properties. Spectral indices enhance the accuracy of water quality assessments and prediction models Table 2.

Table 2. Spectral indicators will help improve water quality and forecast models.

Index	Formula	Reference
Normalized Difference Water Index (NDWI)	G_{L9} - NIR_{L9}) / (G_{L9} + NIR_{L9})	[22]
Modification of Normalized Difference Water Index (MNDWI)	(G_{L9} - $SWIR1_{L9}$) / (G_{L9} + $SWIR1_{L9}$)	[22]
Normalized Difference Moisture Index (NDMI)	(NIR_{L9} - $SWIR1_{L9}$) / (NIR_{L9} + $SWIR1_{L9}$)	[23]
Automated Water Extraction Index (AWEI)	4(G_{L9} - $SWIR2_{L9}$) – (0.25 NIR_{L9} + 2.75 $SWIR1_{L9}$)	[24]
Water Ratio Index (WRI)	(G_{L9} + R_{L9}) / (NIR_{L9} + $SWIR1_{L9}$)	[25]
Normalized Difference Vegetation Index (NDVI)	(NIR_{L9} - R_{L9}) / (NIR_{L9} + R_{L9})	[26]
Ratio Vegetation Index (RVI)	NIR_{L9} / R_{L9}	[27]
Infrared Personage Vegetation Index (IPV)	NIR_{L9} / R_{L9} + NIR_{L9}	[28]
Different vegetation index DVI	NIR_{L9} - R_{L9}	[29]

2.4. Analysis of statistical

SPSS version 25 was used to conduct statistical analysis to determine the associations between OLI-2 band reflectance data from sample sites and water parameters (TOM, TSS, chlorophyll-a, TDS, and turbidity) throughout the winter and spring of 2024. The relationship between Landsat-9 OLI-2 image and parameters of water quality was determined using MLR data and Pearson correlation. A Pearson matrix was created to assess the degree of association between the band reflectance values used in this study and water parameters such as TSS, TDS, turbidity, TOM, and chlorophyll-a. Depending on the water quality parameters, the strength of the association varied between bands. The regression model employed is Multiple Linear Regression (MLR), whereby one variable of interest (dependent variable) is predicted by a large number of different predictor variables (independent variables). MLR allows us to determine the relationship between spectral reflectance in several spectral bands and different water quality parameters and thus predict water quality variables. Every spectral band may contain useful data for determining different parameters of water, thus improving accuracy compared to using only one spectral band. Eq. (3) demonstrates the general form of the MLR Model [19], and the root mean square error (RMSE) and standard error (S.E) equations are represented by Eq. 4 and 5. Fig.2 depicts the flowchart of this study.

$$\mathbf{Y_i = P_0 + P_1X_1 + P_2X_2 + \cdots + P_nX_n} \qquad (3)$$

Where: - Y_i= dependent variable (water quality parameters). $P_0, P_1, P_2\ldots, P_n$= coefficients of regression (R^2). $X_1, X_2\ldots, X_n$ = independent variables (spectral reflectance data).

$$\mathbf{S.E = \frac{S.D}{\sqrt{n}}} \qquad (4)$$

Where: - S. D= Standard Deviation. N= number of points in the data set.

$$\mathbf{RMSE} = \sqrt{\frac{\sum_{i=1}^{n}(y_i - \hat{y}_i)^2}{n}} \quad (5)$$

Where: - y_i= actual observed values. $\hat{y}_i$ = the predicted value.

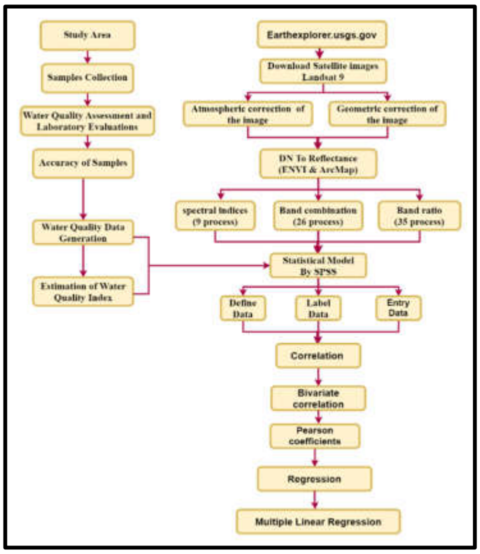

Figure.2. The flowchart of this study.

3. Results and discussion

3.1. Stations Measurements

The biological, physical, and chemical properties of the Tigris River in Wasit are shown in Table 3. In this investigation, station 11 recorded the lowest water temperature (9.91±1.72°C) in the winter, whereas Station 12 recorded the highest mean value (15.8 ± 2.4°C) during the spring season. The water pH at all research locations showed a narrow variance, ranging from (7.37 to 7.98). Water samples' electrical conductivity (EC) varied depending on the research site (it was as high as (1149.67± 13.01 µs/cm) at station 12 in the spring and as low as (913.67 ± 66.6 µs/cm) at station 1 in the winter). Notably, the TDS levels fluctuated at all stations during the research period. The levels ranged from (600 ± 26.45 mg/l) at _station 1 to (743 ± 54.14 mg/l) at station 12. TDS showed higher. values in spring, possibly due to the increased solubility of ions at higher temperatures. TDS and conductivity have a significant association and are frequently associated with inorganic salts [20,22]. According to the current study, station 12 recorded the highest mean water turbidity value (59.15 ± 18.0 NTU) in the spring, while station 2 recorded the lowest mean value (49.04 ± 3.24 NTU) in the winter. We observed that the turbidity number exceeded the WHO critical limit, which should be less than 5 NTU. This is due to agricultural activity, increased winter rainfall, and snowmelt in spring, causing soil erosion that flows into the Tigris River. The turbidity of the Tigris River water fluctuates due to seasonal changes, climate variations, agricultural activities, construction and development, sewage and industrial drainage, and water management and dams [7]. In winter, station 3 had the lowest mean TSS data (42.4 ± 4.42 mg/l), while station 12 had the highest mean value (76.82 ± 28.20 mg/l) in spring. This increase in spring may occur because a large amount of water enters the river, carrying significant quantities of clay due to erosion, gradually increasing the total solids concentration [21].

Table 3. The Average and standard deviation of the environmental factors for the Tigris River during the study period.

Seasons	Stations	Average value ±standard deviation												
		Temp. °C	**PH**	**EC** (µs/cm)	**Turbidity** (NTU)	**TDS** (mg/l)	**TSS** (mg/l)	**TOM** (mg/l)	**T.H** (mg/l)	**DO** (mg/l)	**BOD_5** (mg/l)	**Nitrate** (mg/l)	**phosphate** (mg/l)	**Chlorophyll-a** (mg/l)
Winter	1	10.55±1.04	7.55± 0.2	913.66±66.06	49.49±1.66	600± 26.45	44.5±1.25	1.03±0.097	280± 55.5	10.6±1.11	3.25±0.96	6.13±0.3	0.28±0.052	0.035±0.0036
	2	10.74±1.22	7.73±0.16	1005.66±90.13	49.04±3.24	628.66±31.53	45.33±0.85	1.04±0.098	296.66±10	10.63±0.49	2.64±0.60	6.7±0.9	0.26±0.045	0.036±0.0035
	3	10.26±1.35	7.59±0.53	1035.33±148.13	48.66±2.66	649.66±47.47	42.4±4.42	1.18±0.024	288± 59.5	10.66±0.45	2.63±1.22	6.63±0.45	0.31±0.02	0.0377±0.002
	4	10.42±1.28	7.54±0.22	1010.33±99.4	51.23±1.74	635.33±28.44	42.6±2.34	1.19±0.031	289.33±12.5	10.5±0.75	2.58±0.75	7.06±0.41	0.34±0.030	0.0378±0.0018
	5	10.36±1.65	7.65±0.21	1023.33±116.6	48.36±3.37	657.66±44.73	50.13±1.68	1.27±0.035	271.33±45.9	10.86±0.30	2.64±0.68	6.73±0.65	0.33±0.045	0.048±0.0042
	6	10.35±1.73	7.75±0.28	1024±172.18	47.13±3.42	663± 79.01	47.31±2.41	1.29±0.051	301.66±30	10.26±0.49	2.95±0.93	6.86±0.49	0.28±0.036	0.056±0.0082
	7	10.11±1.77	7.96±0.14	1036± 132.5	49.7±3.56	661.66±65.62	52.50±8.67	1.27±0.015	285.66±47	10.5±0.96	3.05±0.89	7.56±0.61	0.30±0.025	0.044±0.008
	8	10.06±1.90	7.65±0.08	955.33±41.04	49.11±3.76	662±77.27	56.54±2.12	1.31±0.24	280.66±33	10.65±0.48	2.87±0.51	7.83±0.30	0.34±0.045	0.041±0.0017
	9	10.2±1.71	7.49±0.25	993± 93.016	50.58±2.41	674± 53.22	48.99±2.81	1.32±0.038	298.66±54	11.51±0.26	3.21±0.69	7.93±0.45	0.28±0.01	0.042±0.0041
	10	10.27±1.91	7.37±0.098	1042.66±125.18	52.41±1.05	700.66±50.81	55.91±10.26	1.35±0.031	317.33±59.9	11.23±0.33	3.50±0.61	7.7±0.95	0.29±0.03	0.052±0.0076
	11	9.91±1.72	7.74±0.096	1150.33±190.07	54.2±1.86	732.33±52.34	56.15±8.16	1.36±0.23	278.66±42.5	11.67±0.22	3.30±0.67	8.56±0.41	0.35±0.015	0.051±0.0018
	12	10.27±1.82	7.95±0.15	1148.33±189.69	54.65±1.78	743±54.04	57.66±9.72	1.38±0.015	334.66±62	11.22±0.22	3.56±0.72	7.96±0.72	0.28±0.02	0.047±0.0089
Spring	1	13.96±2.4	7.67±0.19	954± 62.98	52.51±14.09	622.66±32.02	64.966±21.2	1.35±0.097	258±73.91	10.89±0.67	2.01±0.37	6.22±1.23	0.23±0.075	0.040±0.0025
	2	14.03±2.55	7.663±0.11	980.33±48.41	55.39±16.04	637.33±29.73	65.20±21.3	1.39±0.037	272.33±80.4	10.50±0.76	2.2±0.30	6.34±1.01	0.24±0.058	0.042±0.0031
	3	14.2±2.55	7.63±0.009	1013.66±60.07	53.13±15.44	665.33±37.20	67.03±22.8	1.40±0.109	274±53.56	10.32±0.67	2.12±0.15	6.57±0.79	0.25±0.09	0.043±0.0014
	4	14.23±2.3	7.75±0.007	1024±41.79	54.16±15.05	664.66±21.54	63.79±17.94	1.42±0.153	283±66.64	10.31±0.29	2.27±0.12	6.64±2.02	0.24±0.075	0.0439±0.0029
	5	14±2.30	7.77±0.11	1044.66±46.45	55.57±15.9	677.66±34.23	65.76±20.14	1.49±0.143	287.33±73.5	9.90±0.24	2.24±0.32	7.32±1.66	0.27±0.072	0.0431±0.0042
	6	14.56±2.5	7.85±0.009	1081.66±47.42	57.1±16.5	690±32.44	68.66±23.78	1.56±0.180	300±73.91	9.59±0.16	2.16±0.32	7.24±0.72	0.29±0.079	0.0483±0.0047
	7	14.4±2.40	7.77±0.13	1073±35.15	57.23±16.4	677.33±17.61	70.03±24.75	1.61±0.186	306±64.5	9.77±0.4	1.86±0.10	6.87±0.70	0.25±0.056	0.051±0.0074
	8	14.83±2.4	7.83±0.08	1083.66±47.08	56.62±17.14	696.33±30.43	72.44±26.27	1.62±0.120	300.66±65.5	9.63±0.89	2.13±0.28	7.27±1.14	0.22±0.051	0.049±0.0056
	9	15.06±2.45	7.83±0.07	1072.66±31.56	54.62±17.17	682.66±30.74	68.52±22.65	1.58±0.104	307.66±56.5	10.38±0.25	2.27±0.28	7.36±1.05	0.27±0.049	0.0496±0.0098
	10	15.2±2.55	7.81±0.04	1124.33±5.50	56.91±18.43	710±21.28	71.07± 23.5	1.66±0.121	304.66±61.6	10.16±0.61	2.36±0.27	7.04±1.08	0.24±0.055	0.053±0.0078
	11	15.6±2.4	7.98±0.12	1128.33±8.73	57.69±17.7	725.66±12.50	73±25.26	1.69±0.154	317.66±60.5	9.54±0.77	2.29±0.40	7.92±0.81	0.27±0.056	0.0552±0.0075
	12	15.8±2.36	7.92±0.05	1149.66±13.01	59.14±18	733.33±10.78	76.82±28.2	1.72±0.089	318.33±66.2	9.27±0.62	2.23±0.42	7.47±1.12	0.30±0.055	0.0554±0.0083

During the winter, Station 11 recorded the highest mean value of (11.67±0.22 mg/l), while during the spring, Station 12 recorded the lowest mean value of (9.27±0.62 mg/l). This variation is because gases become less soluble as water temperature increases. Additionally, the BOD_5 levels varied from (2.01±0.37 mg/l) at station 1 in spring to (3.56±0.72 mg/l) at station 12 in winter. The nitrate levels ranged from (6.13±0.30 mg/l) at station 1 to (8.56±0.41 mg/l) at station 11, with no significant variation in the sampling period. Reactive phosphates reached a maximum mean value of (0.35±0.0152 mg/l) at station 11. during winter and a minimum mean value of (0.22±0.051 mg/l) at station 8 in spring, as per the study findings. The results indicate that, out of the twelve research locations, station 1 had the lowest total organic matter (TOM) content (1.03±0.097 mg/l) in the water sample during winter. In contrast, station 12 had the highest mean value (1.72±0.089 mg/l) in spring. In the spring, station 1 recorded the lowest mean value of water Total Hardness (T.H) at (258 ± 73.91 mg/l), while station 12 recorded the highest mean value in the winter at (334.66 ± 62.08 mg/l).According to the current study, chlorophyll-a concentrations varied, with the lowest mean value (0.035±0.0036 mg/l) recorded at station 1 in winter and the highest mean value (0.055±0.00754 mg/l) recorded at station 12 in spring. With ample sunlight, high temperatures, and nutrients, chlorophyll levels increase during the summer [15].

3.2 Remote sensing results

3.2.1. Turbidity

Remote sensing results indicate that ($SWIR2_{L9}$, MNDWI, NDMI, C_{L9}/B_{L9}, B_{L9}/G_{L9}, and R_{L9}/B_{L9}) are most likely correlated with turbidity in winter. At the same time, in spring (NDMI, C_{L9}/B_{L9}, C_{L9}/G_{L9}, and B_{L9}/C_{L9}) show a significant correlation with turbidity, Table 4 exhibits the correlation between each water quality measure and the Landsat-9 reflectance data.

Table 4. Shows the correlation between each water quality measure and the Landsat reflectance data.

Water quality variables	Image Date			
	6 /January / 2024 (Winter)		4 / April / 2024 (Spring)	
Tur. (NTU)	$SWIR2_{L9}$: 0.560: 0.104	MNDWI: -0.543:0.088	NDMI: -0.568: 0.208	C_{L9}/B_{L9}: -0.530: 0.380
	NDMI: -0.781: 0.17	C_{L9}/B_{L9}: -0.588: 0.017	C_{L9}/G_{L9}: -0.511: 0.529	B_{L9}/C_{L9}: 0.516: 0.335
	B_{L9}/G_{L9}: -0.724: 0.829	R_{L9} /B_{L9}: 0.677: 0.852		
TDS (mg/l)	C_{L9}/B_{L9}: -0.801: 0.055	B_{L9}/G_{L9}: -0.876: 0.511	NDMI: -0.845: 0.001	R_{L9}/GL9: -0.538: 0.034
	R_{L9}/B_{L9}: 0.870: 0.624	R_{L9}/NIR_{L9}: 0.514: 0.249	NIR_{L9}/GL9: -0.529: 0.040	NIR_{L9}/R_{L9}: -0.608: 0.026
	$B_{L9}/NIR_{L9}+C_{L9}$: 0.504: 0.292	$B_{L9}/R_{L9}+R_{L9}$: -0.875: 0.615	$B_{L9}/NIR_{L9}+ NIR_{L9}$: 0.503: 0.016	
TSS (mg/l)	DVI: -0.717: 0.131	$B_{L9}/NIR_{L9}+C_{L9}$: 0.625: 0.067	$SWIR1_{L9}$: 0.564: 0.294	NDMI: -0.678: 0.001
	$B_{L9}+C_{L9}+NIR_{L9}$: -0.528: 0.138	$R_{L9}+C_{L9}$: -0.501: 0.247	G_{L9}/B_{L9}: -0.527: 0.264	R_{L9}/NIR_{L9}:0.503: 0.284
	$B_{L9}+G_{L9}+R_{L9}+NIR_{L9}$: -0.506: 0.079	$B_{L9}/R_{L9}+R_{L9}$: -0.738: 0.008	NIR_{L9}/R_{L9}: -0.541: 0.047	NIR_{L9}/B_{L9}+GL9: -0.528: 0.024
TOM (mg/l)	DVI: -0.513: 0.493	C_{L9}/B_{L9}: -0.849: 0.011	$SWIR1_{L9}$: 0.66: 0.11	NDMI: -0.77: 0.172
	B_{L9}/C_{L9}: 0.845: 0.012	GL9/B_{L9}: 0.72: 0.078	$C_{L9}+NIR_{L9}$: -0.525: 0.128	C_{L9}/B_{L9}: -0.669: 0.165
	R_{L9}/B_{L9}: 0.677: 0.240	$B_{L9}/R_{L9}+R_{L9}$: -0.687: 0.242	B_{L9}/G_{L9}: -0.633: 0.077	NIR_{L9}/C_{L9}: -0.640: 0.148
			$B_{L9}/NIR_{L9}+ NIR_{L9}$: 0.660: 0.152	
Chl-a (mg/l)	C_{L9}/B_{L9}: -0.522: 0.278	B_{L9}/G_{L9}: -0.528: 0.316	NDMI: -0.741: 0.001	B_{L9}/G_{L9}: -0.666: 0.097
	G_{L9}/C_{L9}: 0.576: 0.417	R_{L9}/B_{L9}: 0.625: 0.250	G_{L9}/B_{L9}: 0.661: 0.135	R_{L9}/NIR_{L9}: 0.541: 0.062
	$B_{L9}/R_{L9}+R_{L9}$: -0.641: 0.228		NIR_{L9}/R_{L9}: -0.521: 0.120	$B_{L9}/NIR_{L9}+ NIR_{L9}$: 0.652: 0.006

The term turbidity describes how light in water disperses and absorbs partly rather than travels in upright lines. It is frequently seen as the antithesis of clarity. Since suspended matter is the primary source of water turbidity, fluvial suspended sediment concentrations are commonly determined using turbidity measurement [18]. Figure 3 depicts the distribution of turbidity during the winter and spring seasons of 2024.

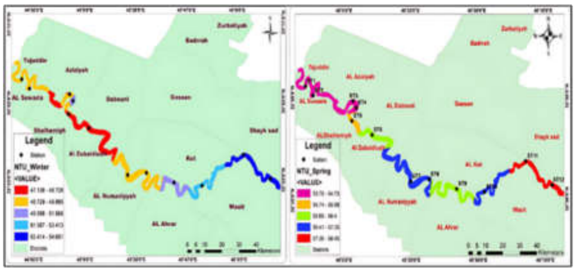

Figure. 3. Map distribution of turbidity during. Winter and Spring.

3.2.2. Total Dissolved Solids (TDS)

According to the multiple regression model used in this study (C_{L9}/B_{L9}, B_{L9}/G_{L9}, R_{L9}/B_{L9}, R_{L9}/NIR_{L9}, $B_{L9}/NIR_{L9}+C_{L9}$, and $B_{L9}/R_{L9}+R_{L9}$) were highly significantly correlated with TDS in winter, while (NDMI, R_{L9}/G_{L9}, NIR_{L9}/G_{L9}, NIR_{L9}/R_{L9}, and $B_{L9}/NIR_{L9}+NIR_{L9}$) in the spring. Both visible and ultraviolet light get absorbed by dissolved substances. Shorter wavelengths, however, have the most significant impact on the volume reflectance spectrum [17]. Furthermore, visible light is absorbed by dissolved materials, remarkably below 500 nm, and the absorbance of these materials rises exponentially with decreasing wavelength [21]. Figure 4 depicts the distribution of TDS during the winter and spring seasons.

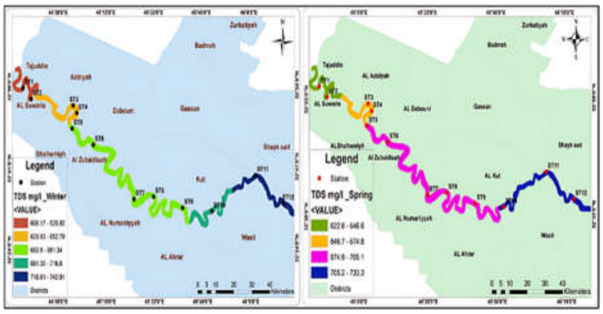

Figure. 4. Map distribution of TDS during. Winter and Spring seasons.

3.2.3. Total Suspended Solids (TSS)

This study indicated that Significant correlations were found between TSS and (DVI, $B_{L9}/NIR_{L9}+C_{L9}$, $B_{L9}+C_{L9}+NIR_{L9}$, $R_{L9}+C_{L9}$, $B_{L9}+G_{L9}+R_{L9}+NIR_{L9}$, and $B_{L9}/R_{L9}+R_{L9}$) in the winter and ($SWIR1_{L9}$, NDMI, G_{L9}/B_{L9}, R_{L9}/NIR_{L9}, NIR_{L9}/R_{L9}, and $NIR_{L9}/B_{L9}+G_{L9}$) In the spring, according to the multiple linear regression model used in this study. Similarly, suspended matter is linked to overall primary production and the transport of heavy metals and micropollutants, making it crucial for maintaining water quality. The primary pollutants found in surface water are suspended materials [22]. In their 2003 study, Ritchie and others highlighted those suspended sediments in the visible and near-infrared regions of the Electromagnetic Spectrum increase the radiance of surface water Figure 5.

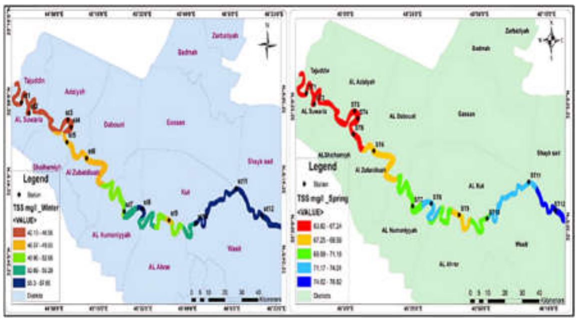

Figure. 5. Map distribution of TSS during Winter and Spring seasons**.**

3.2.3. Total Organic Matter (TOM)

The multiple linear regression model employed in this study indicates a strong correlation between (DVI, C_{L9}/B_{L9}, B_{L9}/C_{L9}, G_{L9}/B_{L9}, R_{L9}/B_{L9}, and $B_{L9}/R_{L9}+R_{L9}$), and total organic matter over the winter season. and ($SWIR1_{L9}$, NDMI, $C_{L9}+NIR_{L9}$, C_{L9}/B_{L9}, B_{L9}/G_{L9}, NIR_{L9}/C_{L9}, and $B_{L9}/NIR_{L9}+ NIR_{L9}$) In spring. TOM absorbs light in the near-infrared region of the Electromagnetic Spectrum. These absorptions can have detectable effects on satellite images [22]. Figure 6 depicts the distribution of TOM during. Winter and Spring seasons.

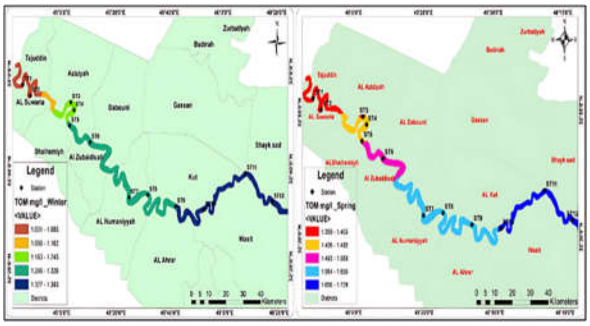

Figure.6. Map distribution of TOM during the Winter and Spring seasons.

3.2.4. Chlorophyll-a (CHL-a)

The OLI-2 ensemble in Landsat-9 demonstrated the highest correlation with chlorophyll-a. Bodies of water containing algae exhibit a specific spectral curve, with significant absorption in the red and green regions and a peak reflectance at the boundary between the red and near-infrared [19]. In this investigation, the multiple linear regression model revealed strong and statistically significant correlations between chlorophyll-a in winter and the variables (C_{L9}/B_{L9}, B_{L9}/G_{L9}, G_{L9}/C_{L9}, R_{L9}/B_{L9}, and $B_{L9}/R_{L9}+R_{L9}$). Similarly, in spring, the variables (NDMI, B_{L9}/G_{L9}, G_{L9}/B_{L9}, R_{L9}/NIR_{L9}, NIR_{L9}/R_{L9}, and $B_{L9}/NIR_{L9}+ NIR_{L9}$) Showed very significant correlations with chlorophyll-a. The elevation of reflectance at (690 nm) relative to the baseline within the wavelength range of (670 to 850 nm) serves as a highly responsive indication of chlorophyll-a concentration [21]. Figure 7 depicts the distribution of chlorophyll-a during. Winter and Spring seasons.

The most suitable regression models are chosen based on the highest values (R^2). Table 5 contains the regression equations for each water quality metric. Our analysis revealed that the use of spectral evidence in this study effectively identifies water features. We achieved this by comparing the situ data with remote sensing data for (TOM, TSS, turbidity, TDS, and chlorophyll-a), as presented in Table 6. Remote sensing offers a complete foretelling of water quality to enhance our understanding of spatial modality and its underlying factors [23]. Consequently, differences in sampling time and sample location precision can lead to discrepancies between the data collected on-site and the data obtained using remote sensing techniques. The paradigm used to analyze the levels of (TOM, TSS, turbidity, TDS, and chlorophyll-a) did not show significant differences from the values recorded in the two study seasons. This is particularly because the difference between the value arrived at through remote sensing and that that is arrived at directly through measurements is very small. This facilitated a thorough evaluation of all study seasons. The strong positive correlation of the coefficient of determination values (R^2), small standard errors (S. E), and low values of RMSE for all the models indicate a high likelihood of accurately predicting all the attributes highlighted in (Table 5) within the scope of this study. The temporal variation of visual image capture also influences the fixed difference in the multiple linear regression equations between the two seasons of the study. This is because we know that the time of year affects the amount of

energy reflected by objects due to differences in the angle of incidence of the sun's rays. This becomes evident when examining the numerical values of some of the constants and elements in the equations [12].

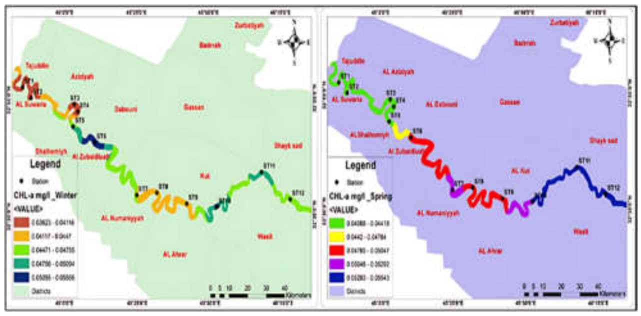

Figure. 7. Map chlorophyll-a distribution during the Winter and Spring seasons.

Table 5. The regression model used in this study for each parameter.

Regression Model in Winter	Regression Model in Spring
Turbidity = 373.401 – ($SWIR2_{L9}$)1095.284 - (MNDWI) 97.703 - (NDMI) 45.571 - (C_{L9}/B_{L9}) 132.297 - (B_{L9}/G_{L9}) 7.883 - (R_{L9}/B_{L9}) 75.780	Turbidity = 626.157- (NDMI)22.801 – (C_{L9}/B_{L9})316.150 - (C_{L9}/G_{L9})31.332 - (B_{L9}/C_{L9}) 238.151
TDS = 11321.356 – (C_{L9}/B_{L9}) 2098.510 – (B_{L9}/G_{L9}) 278.334 – (R_{L9}/B_{L9}) 4300.594 + (R_{L9}/NIR_{L9}) 420.648 – ($B_{L9}/NIR_{L9}+C_{L9}$) 3594.616 – ($B_{L9}/R_{L9}+R_{L9}$) 4747.990	TDS = 4446.554 - (NDMI) 1054.949 – (R_{L9}/G_{L9}) 2653.658 + (NIR_{L9}/G_{L9}) 3519.393 - (NIR_{L9}/R_{L9}) 3906.246 - ($B_{L9}/NIR_{L9}+NIR_{L9}$) 604.669
TSS = 91.566+ (DVI) 933.088 + ($B_{L9}/NIR_{L9}+C_{L9}$) 362.549 + ($B_{L9}+C_{L9}+NIR_{L9}$) 113.765 - ($R_{L9}+C_{L9}$)146.483 - ($B_{L9}+G_{L9}+R_{L9}+NIR_{L9}$) 38.227 - ($B_{L9}/R_{L9}+R_{L9}$) 312.449	TSS = 117.557- ($SWIR1_{L9}$) 115.043 – (NDMI) 118.821 + (G_{L9}/B_{L9}) 15.989 - (R_{L9}/NIR_{L9})14.809 – (NIR_{L9}/R_{L9}) 83.435 + ($NIR_{L9}/B_{L9}+G_{L9}$) 25.887
TOM = 444.043 + (DVI) 2.423 – (C_{L9}/B_{L9}) 182.053 – (B_{L9}/C_{L9}) 228.207 + (G_{L9}/B_{L9}) 2.889 – (R_{L9}/B_{L9}) 24.741 – ($B_{L9}/R_{L9}+R_{L9}$) 28.340	TOM = 35.253- ($SWIR1_{L9}$) 20.081- (NDMI)1.612 + ($C_{L9}+NIR_{L9}$) 3.568 - (C_{L9}/B_{L9}) 9.355 - (B_{L9}/G_{L9}) 6.856 - (NIR_{L9}/C_{L9})11.284 - ($B_{L9}/R_{L9}+R_{L9}$) 6.853
Chl.a = 5.152 + (C_{L9}/B_{L9}) 0.052 + (B_{L9}/G_{L9}) 0.094 + (G_{L9}/C_{L9}) 0.094 – (R_{L9}/B_{L9}) 3.434 – ($B_{L9}/R_{L9}+R_{L9}$) 4.149	Chl.a = 0.601 – (NDMI) 0.127 – (B_{L9}/G_{L9})0.549 - (G_{L9}/B_{L9}) 0.237 + (R_{L9}/NIR_{L9}) 0.074 + (NIR_{L9}/R_{L9}) 0.158 – ($B_{L9}/NIR_{L9}+NIR_{L9}$) 0.026

Table 6. Turbidity, TDS, TSS, TOM, and chlorophyll- measured in situ and by remote sensing, along with corresponding standard error and Multiple linear regression values.

Winter (2024)										
Measured in situ						Remotely sensed				
Station	Turbidity NTU	TDS mg/l	TSS mg/l	TOM mg/l	CHL- a mg/l	Turbidity NTU	TDS mg/l	TSS mg/l	TOM mg/l	CHL- a mg/l
ST1	49.49	600	44.50	1.030	0.0356	49.54	603.14	44.44	1.032	0.0351
ST2	49.04	628.66	45.33	1.040	0.0364	49	627.44	45.51	1.048	0.0413
ST3	48.66	649.66	42.40	1.188	0.0377	49.42	654.99	43.46	1.232	0.0464
ST4	51.23	635.33	42.60	1.195	0.0378	50.69	636.81	42.38	1.181	0.0352
ST5	48.36	657.66	50.13	1.273	0.0484	48.71	638.12	50.14	1.229	0.0444
ST6	47.13	663	47.31	1.293	0.0566	47.17	666.31	50.27	1.270	0.0486
ST7	49.7	661.66	52.50	1.272	0.0446	48.82	664.26	48.35	1.292	0.0467
ST8	49.11	662	56.54	1.314	0.0414	48.99	673.73	56.48	1.303	0.0429
ST9	50.58	674	48.99	1.324	0.0421	51.25	669.69	49.64	1.346	0.0414
ST10	52.41	700.66	55.91	1.355	0.0523	52.22	713.04	55.27	1.377	0.0518
ST11	54.2	732.33	56.15	1.367	0.0514	53.86	723.83	55.97	1.334	0.0509
ST12	54.65	743	57.66	1.383	0.0475	54.87	736.55	58.05	1.374	0.0485
R^2						96%	95%	92%	95%	63%
S. E						0.66	11.6	1.56	0.033	0.0015
RMSE						0.4503	8.4896	1.534	0.0245	0.0040

Spring (2024)										
Measured in situ						Remotely sensed				
Station	Turbidity NTU	TDS mg/l	TSS mg/l	TOM mg/l	CHL- a mg/l	Turbidity NTU	TDS mg/l	TSS mg/l	TOM mg/l	CHL- a mg/l
ST1	52.51	622.66	64.96	1.35	0.0408	53.25	623.82	64.29	1.38	0.0400
ST2	55.39	637.33	65.20	1.39	0.0427	54.78	636.25	65.77	1.385	0.0436
ST3	53.13	665.33	67.03	1.40	0.0430	55.14	674.98	66.49	1.45	0.0448
ST4	54.16	664.66	63.79	1.42	0.0439	54.24	665.12	64.75	1.39	0.0442
ST5	55.57	677.66	65.76	1.49	0.0431	54.48	662.98	65.21	1.44	0.0423
ST6	57.10	690	68.66	1.56	0.0483	56.01	700.05	68.85	1.56	0.0485
ST7	57.23	677.33	70.03	1.61	0.0510	56.95	685.08	71.14	1.61	0.0512
ST8	56.62	696.33	72.44	1.62	0.0499	57.50	696.14	71.94	1.63	0.0506
ST9	54.62	682.66	68.52	1.58	0.0496	57.25	684.14	68.57	1.59	0.0498
ST10	56.91	710	71.07	1.66	0.053	56.77	702.15	70.83	1.66	0.0520
ST11	57.69	725.66	73.003	1.69	0.0552	56.20	718.51	72.53	1.68	0.0553
ST12	59.14	733.33	76.82	1.72	0.0554	57.48	733.87	76.89	1.72	0.0558
R^2						53%	96%	97%	96%	97%
S. E						0.41	9.18	1.11	0.036	0.0014
RMSE						1.2957	6.9967	0.5852	0.0241	0.00077

4. Conclusion

Regarding water quality parameters monitoring in fresh-water bodies such as lakes, rivers, and reservoirs, remote sensing and GIS (represented by satellite images) approaches are more practical, affordable, and effective than in situ methods, which are limited to specific sampling locations. Supervising water quality to help direct conservation efforts and improve the quality of the environment in rivers and lakes is important in determining the state of aquatic systems.

The biological, physical, and chemical parameters of the Tigris River of Wasit are not constant within the river's stretch. Station 11 recorded the lowest water temperature in winter, while Station 12 recorded the highest mean value in spring. The water pH varied from 7.37 to 7.98, and electrical conductivity varied depending on the research site. TDS levels fluctuated at all stations, with higher values in spring due to increased solubility of ions at higher temperatures. Station 3 had the lowest mean TSS data in winter, while station 12 had the highest in spring due to increased clay concentration in river water. Station 12 recorded the highest mean water turbidity value in spring, exceeding the WHO critical limit. DO levels varied between different sites and seasons, with Station 11 having the highest mean value in winter and Station 12 having the lowest in spring. BOD_5 levels varied from Station 1 to 12. The study found no significant variation in nitrate levels between stations, and reactive phosphates reached maximum and minimum values during winter and spring, respectively. Station 1 had the lowest TOM content in winter. In contrast, Station 12 had the highest mean value in spring due to increased sources of sewage, agricultural drainage, and surface runoff. Chlorophyll-a concentrations varied, with the lowest mean value in winter and the highest in spring.

Every metric related to water quality, such as (TDS, turbidity, TSS, TOM, and chlorophyll-a), has an estimated reflectance between (450 and 880 nm). These parameters directly affect the reflection and absorption of light recorded by the satellite sensor. TSS, TDS, and turbidity reduce light reflection. Chlorophyll-a and TOM also absorb light in specific spectral bands. Therefore, Landsat-9 spectral sensors can detect changes in water quality based on spectral reflectance characteristics.

Our study revealed that all bands of Landsat-9 OLI-2 have a significant correlation with water quality parameter measures. The multiple linear regression model and Pearson correlation with band reflections, band ratio, combination band, and spectral indices gave values close to the in-situ results. This correlation highlights the potential of using satellite imagery as a reliable tool for large-scale water quality assessment.

This study shows that the general regression model (multiple linear regression) could be used for all parameters and in all seasons. However, the data collected from different stations differed significantly, leading to different spectral reflectance data. The existence of a general regression model requires a comprehensive study of multiple indicators and flexibility in dealing with diverse data. The measures of water quality, which affect the reflectance, change during the year and are not constant throughout the season; therefore, there is a considerable variance in data gathered from different stations, especially during spring. This seasonal variability makes tracking the incidence and its distribution difficult and indicates the need to create models that would address the need for accurate monitoring.

In this study, we noticed that the water quality parameters of the Tigris River in Wasit Governorate exceed the permissible limit (WHO and Iraqi standards) when the river is heading south due to sewage water flowing into the river, as well as due to agricultural pollutants, solid pollutants, urban sources, and erosion and sedimentation. The enhanced degree of pollution of water resources demands taking urgent measures for the rehabilitation and preservation of this river and its environment and water supply for future generations.

References

[1] W. Ahmed, S. Mohammed, A. El-Shazly, and S. Morsy, "Tigris River water surface quality monitoring using remote sensing data and GIS techniques," *The Egyptian Journal of Remote Sensing and Space Sciences,* vol. 26, no. 3, pp. 816-825, 2023, doi: https://doi.org/10.1016/j.ejrs.2023.09.001

[2] H. J. Jumaah, M. H. Ameen, G. H. Mohamed, and Q. M. Ajaj, "Monitoring and evaluation Al-Razzaza lake changes in Iraq using GIS and remote sensing technology," *The Egyptian Journal of Remote Sensing and Space Science,* vol. 25, no. 1, pp. 313-321, 2022, doi: https://doi.org/10.1016/j.ejrs.2022.01.013.

[3] M. A. Neama, M. Attia, A. Negm, and M. Nasr, "Overview of water resources, quality, and management in Algeria," *Water Resources in Algeria-Part I: Assessment of Surface and Groundwater Resources,* pp. 13-25, 2020, doi: https://doi.org/10.1007/698_2020_522.

[4] M. Jaiswal, J. Hussain, S. K. Gupta, M. Nasr, and A. K. Nema, "Comprehensive evaluation of water quality status for entire stretch of Yamuna River, India," *Environmental monitoring and assessment,* vol. 191, no. 4, p. 208, 2019, doi: https://doi.org/10.1007/s10661-019-7312-8.

[5] N. Al-Ansari, N. Abbas, J. Laue, and S. Knutsson, "Water scarcity: Problems and possible solutions," *Journal of Earth Sciences and Geotechnical Engineering,* vol. 11, no. 2, pp. 243-312, 2021, doi: https://dx.doi.org/10.47260/jesge/1127.

[6] T. Kim and Y. Sheng, "Estimation of water quality model parameters," *KSCE Journal of Civil Engineering,* vol. 14, pp. 421-437, 2010, doi: https://doi.org/10.1007/s12205-010-0421-0.

[7] I. Ahmad, N. I. S. N. Ridzuan, W. N. H. A. W. Hassan, and M. R. R. MAZ, "Water quality monitoring using wireless sensor networks," in *AIP Conference Proceedings*, 2020, vol. 2291, no. 1: AIP Publishing, doi: https://doi.org/10.1063/5.0025040.

[8] C. Östlund, P. Flink, N. Strömbeck, D. Pierson, and T. Lindell, "Mapping of the water quality of Lake Erken, Sweden, from imaging spectrometry and Landsat Thematic Mapper," *Science of the Total Environment,* vol. 268, no. 1-3, pp. 139-154, 2001, doi: https://doi.org/10.1016/S0048-9697%2800%2900683-5.

[9] S. S. Jabar and F. M. Hassan, "Monitoring the Water Quality of Tigris River by Applied Overall Index of Pollution," in *IOP Conference Series: Earth and Environmental Science*, 2022, vol. 1088, no. 1: IOP Publishing, p. 012015, doi: https://doi.org/10.1088/1755-1315%2F1088%2F1%2F012015.

[10] N. Usali and M. H. Ismail, "Use of remote sensing and GIS in monitoring water quality," *Journal of sustainable development,* vol. 3, no. 3, p. 228, 2010, doi: https://doi.org/10.5539/jsd.v3n3p228.

[11] A.-T. Aymen, Y. Al-husban, and I. Farhan, "Land suitability evaluation for agricultural use using GIS and remote sensing techniques: The case study of Ma'an Governorate, Jordan," *The Egyptian Journal of Remote Sensing and Space Science,* vol. 24, no. 1, pp. 109-117, 2021, doi: http://dx.doi.org/10.1016/j.ejrs.2020.01.001.

[12] A. A. Al-Fahdawi, A. M. Rabee, and S. M. Al-Hirmizy, "Water quality monitoring of Al-Habbaniyah Lake using remote sensing and in situ measurements," *Environmental monitoring and assessment,* vol. 187, pp. 1-11, 2015, doi: https://doi.org/10.1007/s10661-015-4607-2.

[13] USGS, " General introduction for the "National Field Manual for the Collection of Water-Quality Data"," in "Techniques and Methods," Reston, VA, Report 9-A0, 2018. [Online]. Available: https://pubs.usgs.gov/publication/tm9A0

[14] S. Marianthi, C. Eleni, and K. Eleni, "Monitoring Lake Ecosystems Using Integrated Remote Sensing/Gis Techniques: An Assessment in the Region of West Macedonia Greece," in

Environmental Monitoring: IntechOpen, 2011.

[15] M. J. Issa, B. S. Al-Obaidi, and R. I. Muslim, "Evaluation of some trace elements pollution in sediments of the Tigris river in Wasit governorate, Iraq," *Baghdad Science Journal,* vol. 17, no. 1, pp. 9-22, 2020, doi: https://doi.org/10.21123/bsj.2020.17.1.0009.

[16] USGS. "United States Geological Survey, Earth Explorer." https://earthexplorer.usgs.gov (accessed.

[17] W. H. Organization, "Guidelines for drinking-water quality: first addendum to the fourth edition," 2017.

[18] USGS. "United States Geological Survey, Landsat Missions." https://www.usgs.gov/landsat-missions/landsat-9 (accessed.

[19] A. J. Al-Fartusi, M. I. Malik, and H. M. Abduljabbar, "Utilizing Spectral Indices to Estimate Total Dissolved Solids in Water Body Northwest Arabian Gulf," *ILMU KELAUTAN: Indonesian Journal of Marine Sciences,* vol. 28, no. 3, pp. 217-224, 2023, doi: https://doi.org/10.14710/ik.ijms.28.3.217-224.

[20] J. Martin, F. Eugenio, J. Marcello, A. Medina, J. A. Bermejo, and M. Arbelo, "Atmospheric correction models for high resolution WorldView-2 multispectral imagery: a case study in Canary Islands, Spain," in *Remote Sensing of Clouds and the Atmosphere XVII; and Lidar Technologies, Techniques, and Measurements for Atmospheric Remote Sensing VIII*, 2012, vol. 8534: SPIE, pp. 153-162, doi: https://doi.org/10.1117/12.974564.

[21] T. Mushtaq, A. Mustafa, R. Rania, A. Hala, Y. Mohammed, and A. Abdul-Lateef, "Change detection for urban expansion in Baghdad City Al-Doura area using geographic information systems," *Nigerian Journal of Technology,* vol. 43, no. 3, pp. 490-498, 2024.

[22] P. Morcillo-Pallarés *et al.*, "Quantifying the robustness of vegetation indices through global sensitivity analysis of homogeneous and forest leaf-canopy radiative transfer models," *Remote Sensing,* vol. 11, no. 20, p. 2418, 2019, https://doi.org/10.3390/rs11202418.

[23] K. Zhang, B. Thapa, M. Ross, and D. Gann, "Remote sensing of seasonal changes and disturbances in mangrove forest: a case study from South Florida," *Ecosphere,* vol. 7, no. 6, p. e01366, 2016, doi: https://doi.org/10.1002/ecs2.1366.